Super resolution imaging of spatial heterogeneities in model thermosensitive hydrogels with implications for their origins

Gopal S. Kenath, Apostolos A. Karanastasis, and Chaitanya K. Ullal*

Department of Materials Science and Engineering, Rensselaer Polytechnic Institute, 110 8th Street, Troy, New York 12180, USA

E-mail: ullalc@rpi.edu

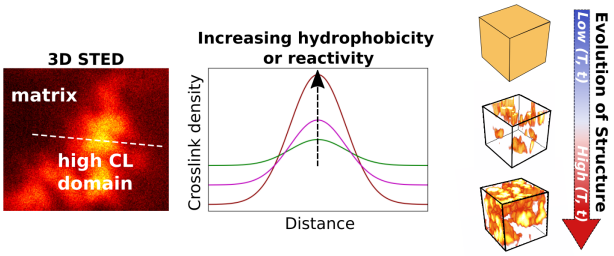

Abstract

Three dimensional nanoscale crosslink density variations are an important and incompletely understood morphological aspect of polymer gels. Here, within the context of establishing a deeper understanding of these so called spatial heterogeneities, we study the spatial distribution of dye tagged acrylamide monomers in bulk thermosensitive PNIPAM gels using a combination of 3D STED and multicolor confocal microscopy. We identify consistent microstructural trends for the various dye tagged monomers, thereby expanding the prevailing picture of spatial heterogeneities in thermosensitive gels. Specifically, we provide new morphological insights into the distribution of crosslinks, the nature of the interface that defines the polymer rich regions, and the incidence and connectivity of higher crosslink density regions as a function of quench time and preparation temperature. While, phase separation and reactivity rate constant differences have only been studied in isolation as the dominant cause of spatial heterogeneities in thermosensitive gels, our results show that both phenomena play an important role in determining crosslink density distributions.

Introduction

Polymer network gels are known to exhibit inhomogeneities on several length scales.[1] The inhomogeneities that extend to and dominate the largest of these length scales arise due to the non-uniform spatial distribution of cross-links in the network during the polymerization process. These so called spatial heterogeneities impact the macroscopic properties of the gel, particularly in terms of the material's mechanical properties, permeability and optical clarity, which raises the importance of unambiguously establishing the spatial variation of crosslink distributions.[2] Much of our understanding of the structure of spatial heterogeneities comes from scattering studies.[3–21] However, the ensemble averaged nature of scattering obscures important structural detail. Thus, the direct three dimensional visualization of gels in their swollen state, with nanoscale resolution remains an important goal in closing the knowledge

gap associated with these important network defects.

The most notable success in the direct three dimensional visualization of gels in this regard is the application of Laser Scanning Confocal Microscopy (LSCM) to the study of heterogeneous poly(N-isopropylacrylamide), or PNIPAM, gels,[22,23] a system in which the presence of spatial heterogeneities can be very pronounced. In these landmark studies, PNIPAM gels were stained by physisorption of a hydrophobic dye and imaged by LSCM. To compensate for the diffraction limited resolution of LSCM, the microscopy was complemented by small angle neutron, ultrasmall angle neutron, and light scattering data.[23] Structures have been identified for relatively low and high polymerization temperatures, respectively. At lower polymerization temperatures, spatial heterogeneities are negligible. At higher polymerization temperatures the resultant gel is described as being a hierarchical, sponge-like structure, constituted by two bicontinuous phases. The polymer rich phase is described as consisting of a bimodal distribution of mesh sizes, with tightly cross-linked 'microgels' uniformly distributed in a more loosely crosslinked network of water swollen polymer chains. The second phase is described as being mostly composed of water, and the interface is implied to be sharp and well defined. For the purposes of this paper, we will refer to these structural descriptions as the "2008 LSCM" model. Imaging of spatial heterogeneities at intermediate times and intermediate polymerization temperatures has not been reported, although spectroscopic studies[24] have been used to provide insight into the polymerization process.

While information from LSCM studies have clearly served to undergird the prevailing model of crosslink distributions in PNIPAM gels, there remain limitations on the extent to which structural insights can be derived from this implementation of fluorescence microscopy.[25] The most restrictive of these limitations is associated with the resolution of the instrument, and to a lesser degree, labelling inefficiencies of the fluorescent probe. For high numerical aperture systems and visible wavelengths, the resolution of LSCM is $\sim$200nm laterally and $\sim$600nm axially. Imaging water swollen gels results in further degradation of

the resolution due to the refractive index of water (∼1.3). Such resolutions are particularly constraining in the case of PNIPAM gels, where structural manifestations of spatial heterogeneities often range from tens of nanometers to tens of microns. Additionally, the use of physisorbed dyes for labeling in these studies is subject to inefficiencies that include being potentially diffusion limited, stochastic in nature, and not directly related to the density of multifunctional monomers. Taken together, this implies that important structural details associated with the three dimensional distribution of spatial heterogeneities remains to be established.

Closely tied to the structure of spatial heterogeneities is their origin within polymer networks, the explanations for which have been summarized[2] as conforming to one of three conceptual pictures. Spatial heterogeneities are described as resulting from: (i) differences in monomer and cross-linker reaction rate kinetics,[26] (ii) frozen thermodynamic concentration fluctuations[20,27] or (iii) chain overlap at cross-linking.[28,29] These pictures have been variously validated through experimental studies that correlated the impact of process parameters such as preparation temperature,[4] reactivities and concentrations of monomers[3,30–33] with the incidence of spatial heterogeneities. Importantly, these correlations were primarily characterized by using macroscopic properties such as turbidity and modulus or increased scattering intensities over certain scattering angle ranges, as opposed to directly imaged structure. The limited studies[24] that directly correlate the impact of process parameters, and therefore the origin of spatial heterogeneities, with structure rely heavily on the aforementioned LSCM studies and are subject to their limitations.

The advent of super resolution microscopy[34] has pushed the limits of resolution of fluorescence microscopy to the length scales relevant to polymer and colloidal systems.[35–38] PNIPAM colloidal gels in particular have benefited from its ability to extract high resolution structural information in the particle's native swollen state.[39–41] Within the specific context of the direct visualization of spatial heterogeneities, an important advance has been the development of fluorescently tagged acrylamide cross-linkers.[42] The power of combining the

labelling specificity of such functional crosslinkers with the diffraction unlimited resolution of super resolution microscopy is exemplified by the finding that individual colloidal PNIPAM gel particles prepared by precipitation polymerization do not have spherically symmetric crosslink distributions[42] as was previously thought.[21]

In this paper, we provide new insight into the structural nature and origins of spatial heterogeneities in bulk gels. This is facilitated by the use of 3D STED microscopy and multi-color LSCM to reveal the spatial distribution of dilute quantities of dye tagged acrylamide monomers in bulk PNIPAM gels. These distributions are impacted by both, the parent hydrogel structure, and the properties of the respective dye tagged crosslinker. A uniquely enabling aspect of the latter is captured in the bottom of Fig 1a; the independent handles of the choice of dye molecule and its associated hydrophilicity, and the chemistry of the acrylamide monomer with its attendant reactivity rate constant, gives us the ability to easily vary the hydrophilicity and reactivity rate constant of the functionalized crosslinkers. This ability, in turn, allows us to directly visualize and disentangle the corresponding impacts of phase separation and consumption kinetics on the spatial distribution of the functionalized crosslinkers.

Fig 1b summarizes our observations of consistent morphological features across the various distributions of the dye tagged monomers. Contrary to the contemporary 2008 LSCM model of the polymer rich domains, we find that the highly crosslinked regions are not uniformly distributed within the polymer rich regions, but instead are more centrally located within these regions. The crosslink density within the polymer rich region is not uniform, but decreases monotonically away from the highly crosslinked regions towards the water rich phase, which is, in contrast, relatively uniform in crosslink density. The crossover from the polymer rich phase to the water rich phase is not associated with a large discontinuous variation in crosslink density. The nature of this interface is relevant to interpretations of the 2008 LSCM model as implying that these gels are nano-porous.

Finally, the evolution of the morphology as a function of polymerization quench time

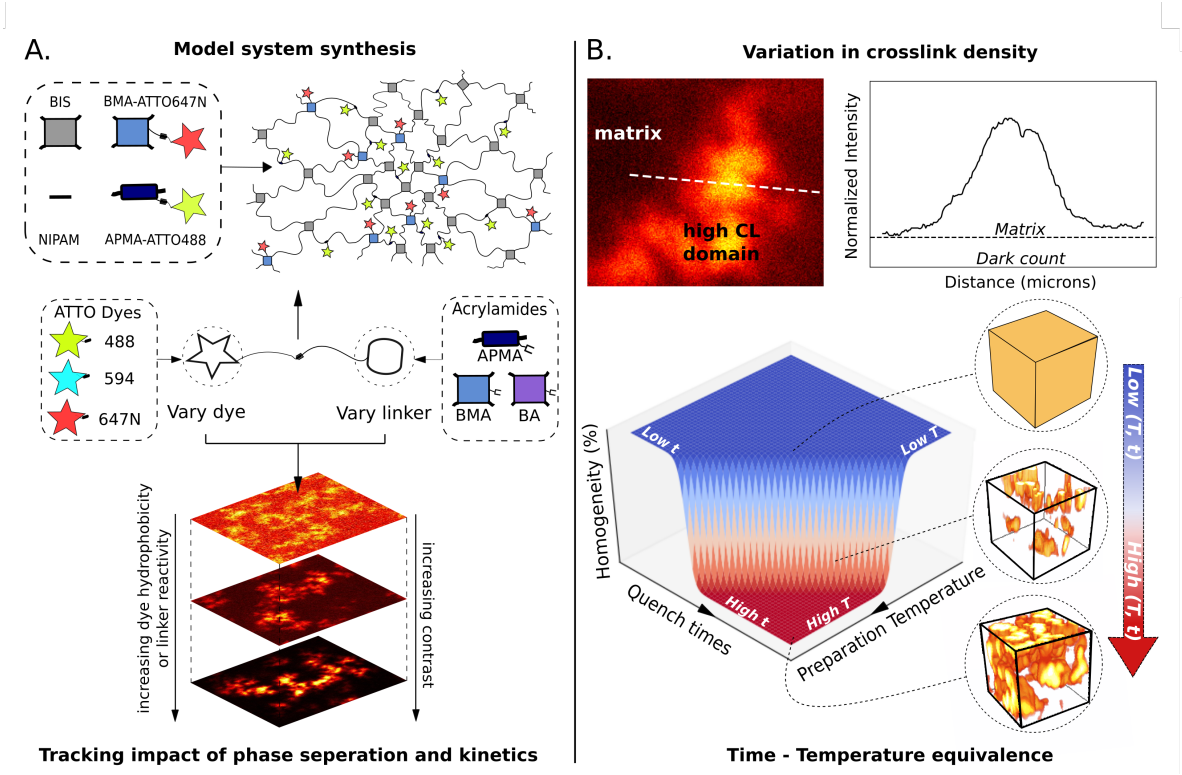

Figure 1: Outline of the study. **(A)** A dilute amount of dye tagged acrylamide monomers are co-polymerized along with the parent monomers (NIPAM and BIS). The distribution of dye tagged monomers within the network reveals that increasing dye hydrophobicity or linker reactivity results in increased localization of dye tagged monomers within the polymer rich domains. **(B)** An improved model of heterogeneous PNIPAM gels that extends beyond the current two phase sponge-like description. Top: Observation of a variation in crosslink density that on average monotonically increases towards the center of the polymer rich heterogeneity, and an interface between the polymer rich heterogeneity and matrix that is not accompanied by a large discontinuity in crosslink density. Bottom: 3D STED imaging reveals an increasing connectivity between spatial heterogeneities with preparation temperature, with bicontinuity observed at high preparation temperatures. A similar trend is observed with quench times, establishing that a sigmoidal evolution of transmittance manifests for quench times as well as preparation temperature.

and temperature of polymerization also reveals new structural insights. We find a progression from homogeneously distributed dye tagged monomers at low temperatures and short polymerization quench times, to formation of discrete regions of high crosslink density embedded within a lighter cross-linked matrix, through to bicontinuous sponge like structures consisting of polymer rich and water rich regions. These observations represent an advance in our understanding of spatial heterogeneities in bulk NIPAM gels for two reasons. First, the morphology of isolated regions of higher crosslink density had not been recorded before.

Second, our results show an equivalence in structural progression between polymerization temperature and polymerization quench times.

Taken together, these morphological insights represent a significant update to the prevailing model of spatial heterogeneities in thermosensitive gels. Our results clearly establish that both phase separation during polymerization and reactivity rate constant differences can play an important role in determining the structure of spatial heterogeneities. These schools of thought on the origin of spatial heterogeneities have typically been reported independently of each other.

Materials and methods:

Materials and reagents:

A detailed list of chemicals and reagents is provided in the SI.

Dye tagged monomer synthesis:

Dye tagged monomers were obtained by reacting the respective monomer bearing a primary amine group with an activated ester of the respective dye. The three dyes used, ATTO488, ATTO 594 and ATTO647N, were purchased (ATTO-TEC GmbH, Germany), and used as received. Three monomers were tagged with dyes. Two of these monomers were multifunctional, N,N'-(2-aminopropane-1,3-diyl)bis(2-methylacrylamide) and N,N'-(2-aminopropane-1,3-diyl)diacrylamide; the third was a bifunctional monomer, N-3-aminopropyl-methacrylamide. Details of the synthesis of the dye tagged mutifunctional monomers have been reported previously.[42,43] The bifunctional monomer was obtained commercially (sigma $\geq$ 99%). We denote the methacrylamide, acrylamide and N-3-aminopropyl-methacrylamide monomers as BMA, BA and APMA respectively. The dye tagged monomers are denoted as monomer-dye, *e.g.* BMA-ATTO647N.

Synthesis of tagged hydrogels for imaging:

Dye functionalized hydrogels were synthesized consistent with the protocol used by Hashimoto *et al.*[22,23] For the synthesis of the tagged gels, 0.264 mmol NIPAM (30 mg); 2.057 μmol(0.317 mg or 17 μL of 1.85 mg/ml in water) of N,N'-Methylenebis(acrylamide), henceforth referred to as BIS; 4.114 nmol of each dye tagged acrylamide monomer added; and 160.8 μL water were mixed in a 1.5 mL microcentrifuge tube and cooled down to 0^oC. TEMED (1 μL) and APS (4.2 μl of 38.4 mg/ml solution) were added to the reaction solution, followed by thorough mixing, still at 0^oC. 35 μL of the reaction mixture is dropcast in a well, formed by sticking a Grace Bio-Labs SecureSeal imaging spacer (13 mm inner dia x 0.12 mm thick) onto a coverslip (#1.5) cleaned in triplicate with acetone, ethanol and DI water. The monomer solution in the well is sealed with another coverslip (#1.5), cleaned in hot piranha solution. This coverslip configuration is then secured in a sealed chamber (Presslok demountable chamber, Sigma-Aldrich), and placed in a water bath maintained at a given preparation temperature. After 1 hour, the piranha cleaned coverslip is prised off and 200 μL of DMSO is dropcast onto the hydrogel, and left to sit for 15 minutes to let the hydrogel exchange solvents and swell in DMSO. The excess DMSO was removed and the hydrogel was then mounted onto a standard glass slide and imaged using LSCM and STED microscopy.

STED and LSCM imaging:

Image acquisition:

LSCM and STED images were acquired with a Leica TCS SP8 STED microscope. Although the application of 3D STED microscopy to the imaging of 3D nanostructured colloidal and polymeric structures has been reported as early as 2008,[35,36] familiarity of the technique within the polymer community is still not widespread. For the convenience of the reader, a brief description of pertinent aspects of 3D STED microscopy via a single lens is included in the SI, while the more specific experimental details are presented in this subsection. The

SP8 microscope is equipped with a white light laser (WLL) for excitation and three depletion lasers: two continuous wave lasers at 592 nm and 660 nm and a pulsed laser at 775 nm. A 63X 1.3NA glycerol lens in conjunction with the hybrid detector was used to acquire images. DMSO was chosen as the imaging solvent as it is a good, aprotic solvent that has a similar refractive index to the immersion medium of the glycerol lens used. A correction collar on the lens was used to compensate for residual spherical aberrations. The Leica Application Suite X (LAS X) was used as a software platform, with the scan speed set at 400Hz (400 lines/s). The excitation wavelength and the detection windows were set in accordance with the dye being visualized.

For LSCM imaging, a 150x150μm^2 area was imaged with the image size set at 4096x4096 pixels and 1% of the maximum power of the WLL laser (1.5mW) introduced into the excitation channel. For an excitation wavelength of 647nm this resulted in point spread functions with FWHM of $\sim$270nm in the focal plane and $\sim$670nm along the optical axis. 3D STED images of 20x20x10μm^3 subvolumes were constructed from 100 slices, with each slice comprised of 1024x1024 pixels. During 3D STED imaging, 3% of the maximum power of the WLL laser (1.5mW) was introduced in the excitation channel and 40% and 60% of the maximum power of the depletion (1.5W) laser was introduced into the xy and z donuts respectively. The resultant STED point spread functions were measured to be $\sim$100nm in the focal plane and $\sim$150nm along the optical axis for the ATTO 647N dye.

Image visualization:

The 3D images in the paper were constructed using Imaris imaging software. The images were thresholded to selectively visualize the high crosslink density domains. The threshold was typically set to be just above the average intensity exhibited by the surrounding matrix regions.

Synthesis of pristine gels for transmittance measurements:

Pristine bulk hydrogels were synthesized as per the protocol reported by Hashimoto *et al.*[22,23] 150 mg NiPAM (1.32 mmol), 1.585 mg (10.285 μmol, 85 μL of 1.85 mg/ml) BIS and 889 μL water were mixed in 1.5 mL microcentrifuge tube and cooled down to 0^oC. TEMED (5 μl) and APS (21 μl of 38.4 mg/ml solution) were added to the reaction solution, followed by thorough mixing, still at 0^oC. The monomer solution was loaded in a sealed chamber (Presslok demountable chamber, Sigma-Aldrich), using a Viton O-ring spacer (1.5 mm) for the confinement of the monomers between 25 mm circular #1 coverslips (VWR), both of which had been cleaned in hot piranha solution. The holder was subsequently placed in a thermostated water bath at the desired temperature for 1 hour. The hydrogel stub was then stored in DI water overnight for it to reach swelling equilibrium.

Transmittance measurements:

Transmittance measurements were taken using a 640nm laser source (Picoquant PDL 800-D/LDH DC 640) and power meter (Newport 2931-C). Hydogel stubs were placed between the source and the detector and transmittance was estimated as the ratio of the signal detected after and before placing the stub in the path. Dark background was measured $\sim$ 20nW and 100% transmittance was set at $\sim 15\mu$W.

Results and discussion:

To gain insight into the structure and origins of spatial heterogeneities within model PNIPAM bulk hydrogels, dye tagged monomers were introduced in trace amounts along with the standard NIPAM and BIS monomers. The chosen dyes enabled 3D super resolution and multicolor confocal microscopy imaging of the dye tagged monomer distributions within the network. As was noted in the introduction, it is known that the spatial distribution of monomers in PNIPAM networks can be strongly impacted by differences in their reaction

rate constants, as well as the tendency of precursor chains to phase separate during the initial stages of the polymerization process. The BMA, BA and APMA monomers possess three distinct sets of kinetic reaction rate constants with which the dye tagged monomers are incorporated within the network.[43] Separately, the dyes used exhibit different degrees of hydrophobicity,[44] which in turn, impacts the degree of hydrophobicity that a given dye tagged monomer exhibits. The structures of the monomers and dyes used are shown in Figure 2. This ability to control, almost independently, the hydrophobicity and the reactivity of the dye tagged monomers is important, as it enables direct visualization of the impact of phase separation and reactivity rate constants on the spatial distribution of the dye tagged monomers within the gel network.

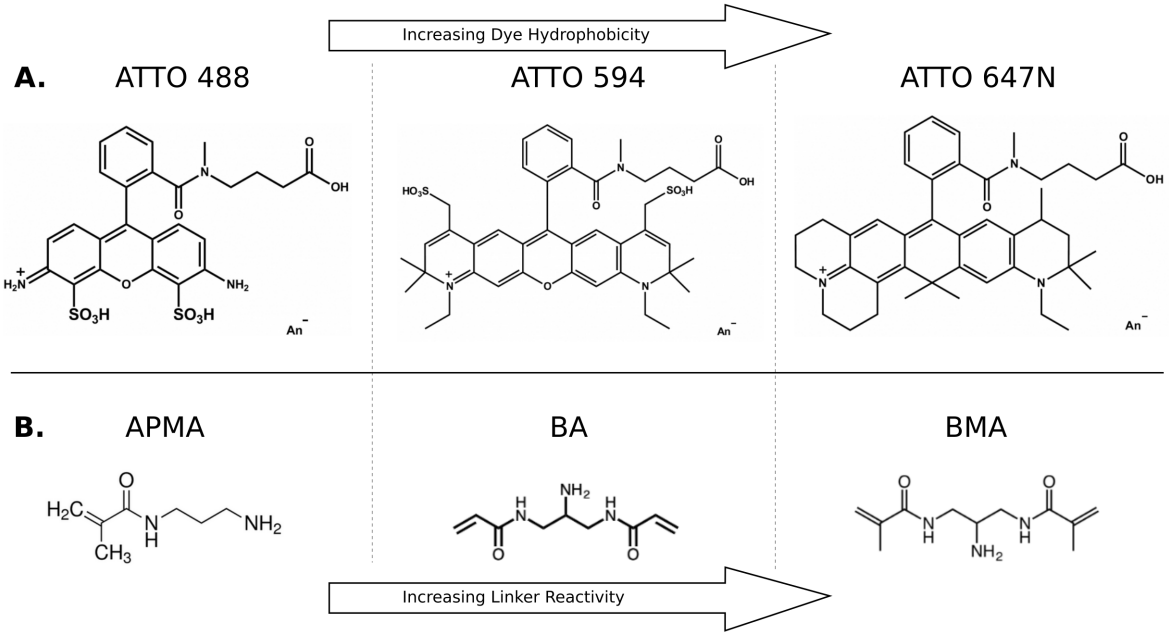

Figure 2: **(A)** Chemical structures of the dyes used in this study arranged in order of increasing hydrophobicity. **(B)** Chemical structures of the linkers used in this study arranged in order of increasing reactivity.

Figure 3 captures the impact on the spatial distribution of the dye tagged monomer while selectively varying the dye and the monomer reactivity, respectively. The top row of Figure 3 shows one channel of multicolor LSCM images of dye tagged BMA monomers from three different gels, each prepared at 27^{o}C with a different dye. As expected for this preparation

temperature, the images reveal phase separated polymer rich and water rich regions, the latter of which we refer to as 'matrix', hereon. The preferential localization of the dye and therefore the contrast between the polymer rich regions and the matrix increases as the dye is varied from BMA-ATTO488 through BMA-ATTO594 to BMA-ATTO647N. Fig 3(E) allows for quantitative comparison of the contrast across dyes as it shows intensity variations along specific line profiles, in which the intensities are normalized by the average intensity associated with the respective matrix regions. This progression in preferential localization is the same sequence in which the hydrophobicity of the dyes increases.[44] Given that acrylamide chemistry (BMA) and preparation temperature ($T_p = 27^oC$) are the same for these three samples, we ascribe the increase in selectivity of the dye distributions primarily to the trend in hydrophobicity of the dyes. This conclusion is further strengthened by the observation of the same trend in dye tagged monomer distributions obtained for APMA functionalized by the same set of dyes. The overlay of the two channels and a comparison of the APMA distributions are shown in the supplementary information.

On the other hand, the left column of Figure 3 exemplifies the impact of varying acrylamide chemistry, and therefore consumption rate kinetics, on the distribution of ATTO-647N tagged multifunctional monomers. Previously, the BA variant was reported to exhibit slower consumption kinetics in comparison to the BMA variant in PNIPAM colloidal gel systems.[43] A similar impact on labeling is observed here, with the contrast between the phase separated domains and the matrix decreasing from the BMA-ATTO647N to the BA-ATTO647N distributions. Lower reaction rates lead to reduced incorporation of the respective monomer into PNIPAM chains that phase separate during the initial stages of the reaction and form the polymer rich heterogeneities of the network. The lower contrast between the polymer rich regions and the matrix exhibited by tagged monomers that exhibit lower hydrophobicities and/or reaction rates is also accompanied by a reduction in contrast observed between features within the polymer rich heterogeneities.

The spatial distribution of any given functional monomer is impacted not just by the

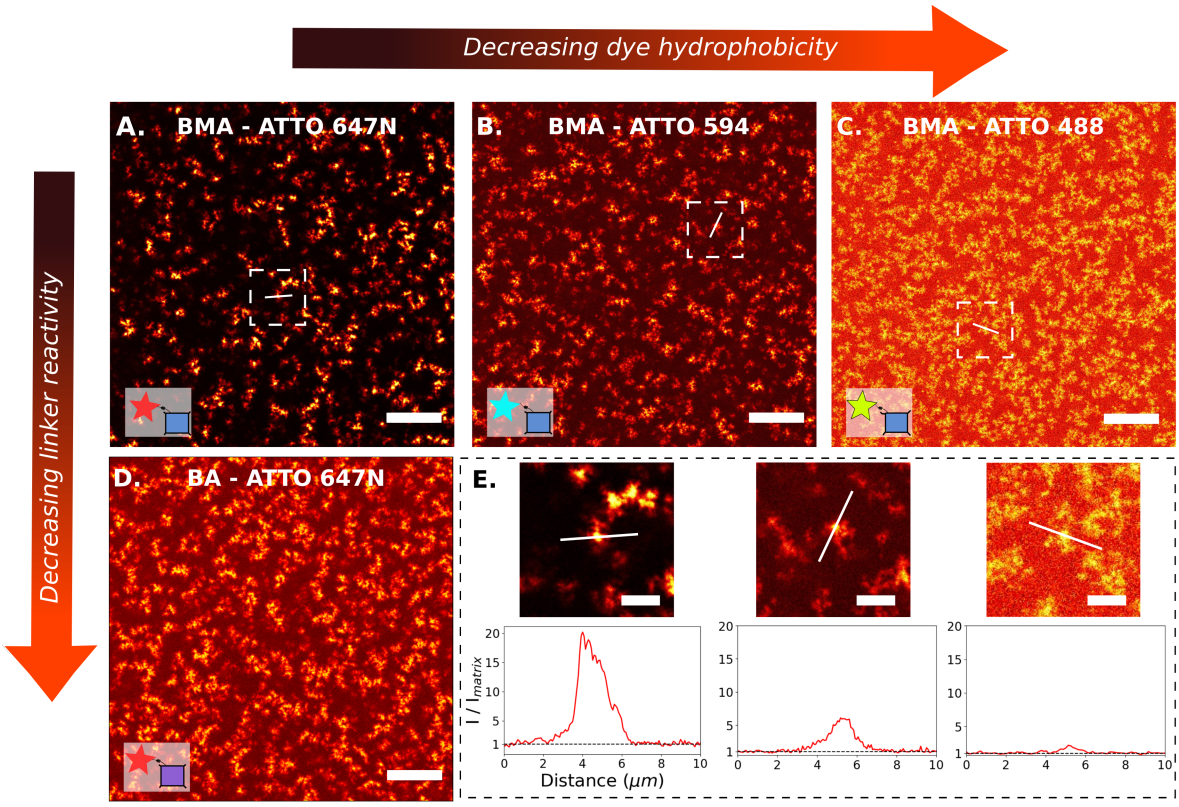

Figure 3: Independently varying the dye, and therefore its hydrophobicity, and the acrylamide chemistry, and therefore monomer reactivity, disentangles the impact of phase separation and reactivity kinetics on dye tagged monomer distribution. **(A), (B) and (C)** Decreasing dye hydrophobicity, from ATTO647N to ATTO488, while using the same acrylamide monomer (BMA) results in lower contrast between the polymer rich regions and the matrix as well as lower contrast between features of the polymer rich regions. **(A) and (D)** Decreasing the acrylamide reactivity, from BMA to BA, while using the same dye (ATTO647N) has a similar impact. The intensity in each image is normalized to the average matrix signal of the respective image, while color bars scale between zero and the maximum of the respective images. **(E)** Top row: Higher magnification images of the sub-regions demarcated in (A), (B) and (C). Bottom row: Intensity variations relative to the respective average intensity associated with the matrix along the indicated line profiles. Preparation temperature for all gels in figure is $T_P = 27^oC$. Scale bars in (A), (B), (C) and (D) are equal to 20μm. Scale bars in (E) are equal to 5μm

.

specific properties of the respective dye tagged monomer, but the parent hydrogel structure as well. Figure 4, which shows the spatial distribution of two distinct functional monomers, BA-ATTO647N and BMA-ATTO488, within the same region of a gel, exemplifies this phenomenon. While the exact distributions differ, common features are evident, for example, the location of the interface between the polymer rich regions and the matrix. This morpho-

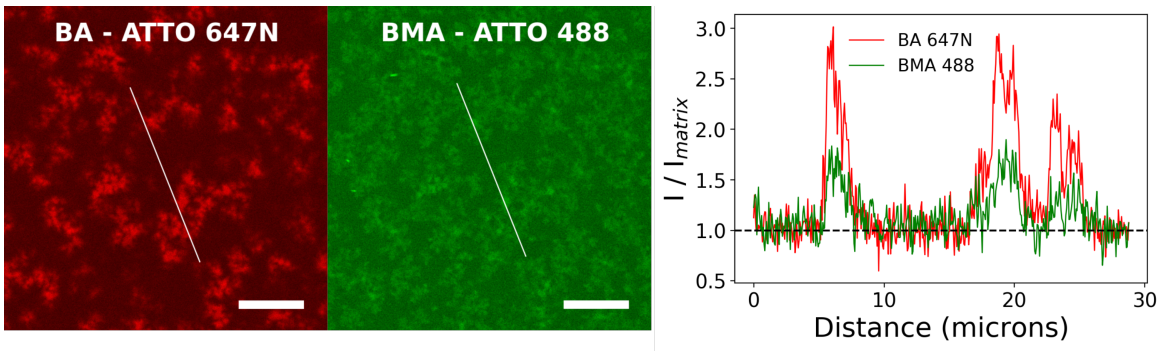

Figure 4: Left: Two separate color channels showing the distribution of BA-ATTO647N (shown in red) and BMA-ATTO488 (shown in green) for the same region of a gel that incorporates both dye tagged monomers. Right: Line profiles showing intensity variations relative to the respective average matrix signal. Preparation temperature for the gel in figure is $T_P = 27^oC$. Scale bars are equal to 10μm.

logical signature is seen for other dye tagged monomer combinations as well (see SI). We thus use consistent morphological features across functional monomers, as well as trends in the impact of hydrophobicity and reactivity rate constants on the distribution of the respective monomers to provide insight into the nature of spatial heterogeneities in thermosensitive hydrogels.

Figure 5 shows STED images of BMA-ATTO647N distributions within bulk PNIPAM gels prepared at 27^oC, and highlights the key structural features observed within the sub-structure of spatial heterogeneities. The superior resolution achieved via 3D STED imaging in comparison to Laser Scanning Confocal Microscopy imaging is exemplified in Fig 5A. Fig 5B shows the normalized variation of BMA-ATTO647N monomers in the bottom-most transverse slice of the STED image shown in Fig 5A. This two-dimensional cut and the accompanying line profile reveal that on average, the concentration of dye tagged monomers monotonically decreases from the center of the heterogeneity towards the surrounding matrix phase. This morphological feature manifests for the other dyes and monomers tested in this work (see SI for examples). We also note that the multifunctional monomers used in this work, when dilutely incorporated into colloidal PNIPAM gels prepared by precipitation polymerization, are known to result in ensemble averaged spatial distributions[43] that share the well established sigmoidal functional form of the parent BIS crosslinker.[21] The

characteristics of the individual sigmoidal distributions vary in a manner that is consistent with the respective properties of the tagged multifunctional monomers. The aforementioned consistent trend in the spatial distribution of the tagged monomers in the bulk hydrogel along with the precedent of the colloidal gel particles, allows us to conclude that the parent crosslinker, BIS, will also possess on average a monotonically decreasing trend in crosslinker density within the heterogeneity, albeit with a contrast consistent with its respective consumption kinetics and hydrophobicity. The observed distribution of the higher crosslink density regions within the polymer rich spatial heterogeneities is noteworthy as it deviates from the 2008 LSCM model[22,23] for the structure of PNIPAM bulk gels prepared at 24.5^{o}C and 27^{o}C. There, the polymer-rich phase is described as effectively having a bimodal mesh size distribution, consisting of microgels with highly cross-linked network chains uniformly distributed in a loosely cross-linked network.

The bottom right inset shows the variation of BMA-ATTO647N across the line profile shown in the figure. Consistent with Figures 3 and 4, we denote the region where there is a significant change in slope as the interface between the polymer rich heterogeneities and the matrix. Notably, this change in slope is not accompanied by a discontinuity in the tagged monomer concentration. To gain insight into the connectivity of the various ranges of tagged crosslinker concentration, the normalized intensity distribution was binned into five intensity ranges, with a unique color assigned to each range as shown in the bottom left inset of Figure 5B. Figure 5C depicts the spatial distribution of the intensities that correspond to the ranges [0.2,0.4] and [0.6,1.0] in green and red respectively, within the sub volume of the gel shown in Figure 5A. This color coded image highlights the differences in connectivity between the outer surface of the polymer rich heterogeneities and the more centrally located crosslink rich regions. The outer green envelope shows that the polymer rich regions within the network connect with each other to form a 3D bicontinous network. On the other hand, the regions of highest average functional crosslinker density appear to be disconnected from each other as shown in Fig 5D.

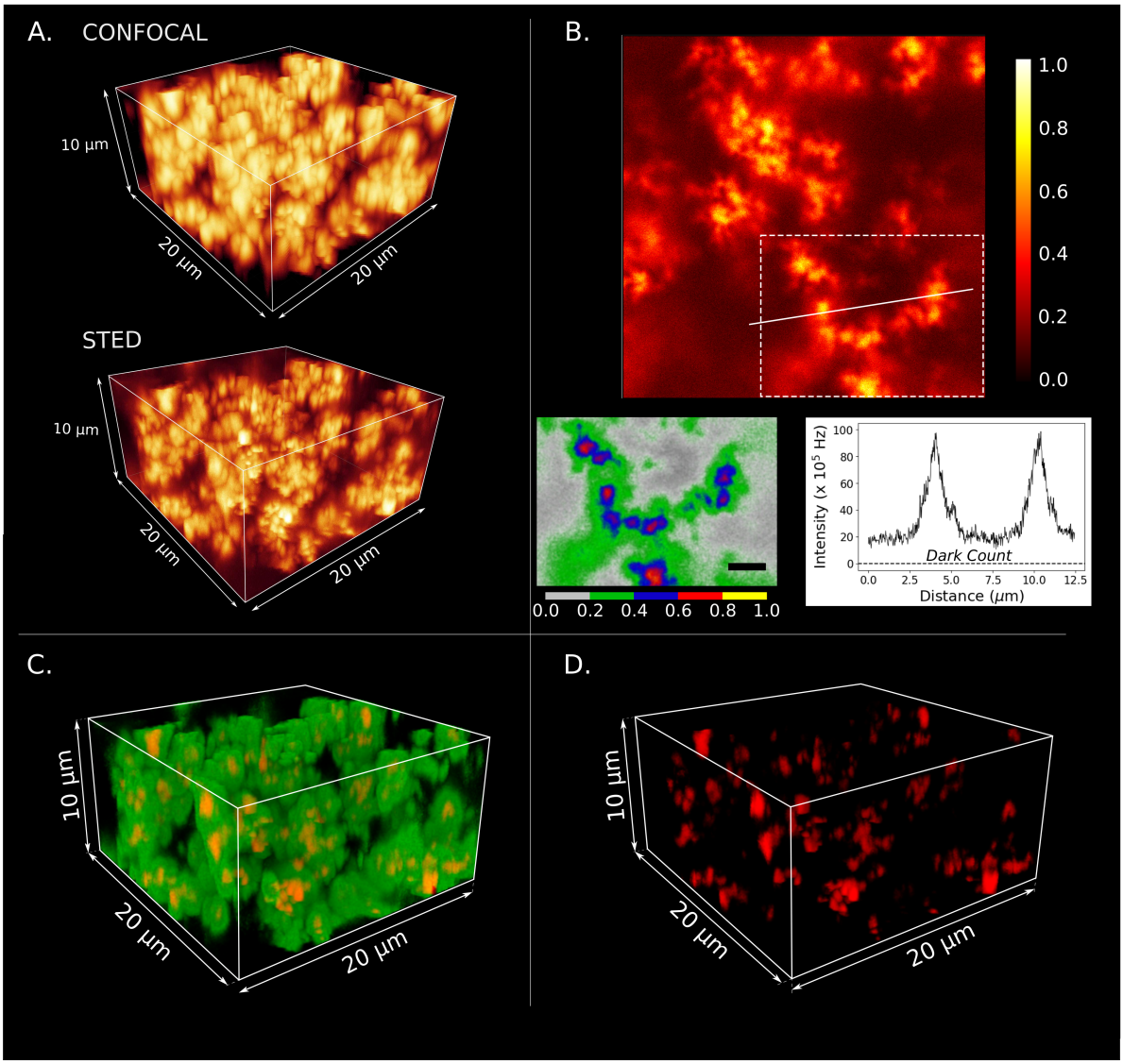

Figure 5: Results from 3D STED imaging of BMA-ATTO647N distributions within PNIPAM bulk gels prepared at $T_p = 27^oC$. **(A)** Comparison between LSCM and 3D STED imaging of the same subvolume within a dye tagged bulk PNIPAM gel. **(B)** Top: Intensity variations within an xy section representing the bottom most section of the volume shown in A. Bottom left: Intensity distributions binned into five intensity ranges to highlight the monotonically decreasing distribution of dye tagged monomers within polymer rich regions. Scale bar is 2μm Bottom right: Intensity variation across a line passing through a heterogeneity and the matrix depicting the interface between the two regions. **(C)** Intensity distributions in 3D subvolume binned as per the scheme in (B), with only the green and red+yellow regions depicted to highlight the differences in the connectivity between the two regions. **(D)** Selective visualization of the high density domains in (C), highlighting the lack of connectivity between these domains.

The new morphological observations summarized in Figure 5 are further strengthened by examining the evolution of the structure of PNIPAM gels at various preparation tem-

peratures, which includes establishing the final morphology of gels prepared at intermediate preparation temperatures. Figure 6 shows images of the final distribution of BA-ATTO647N

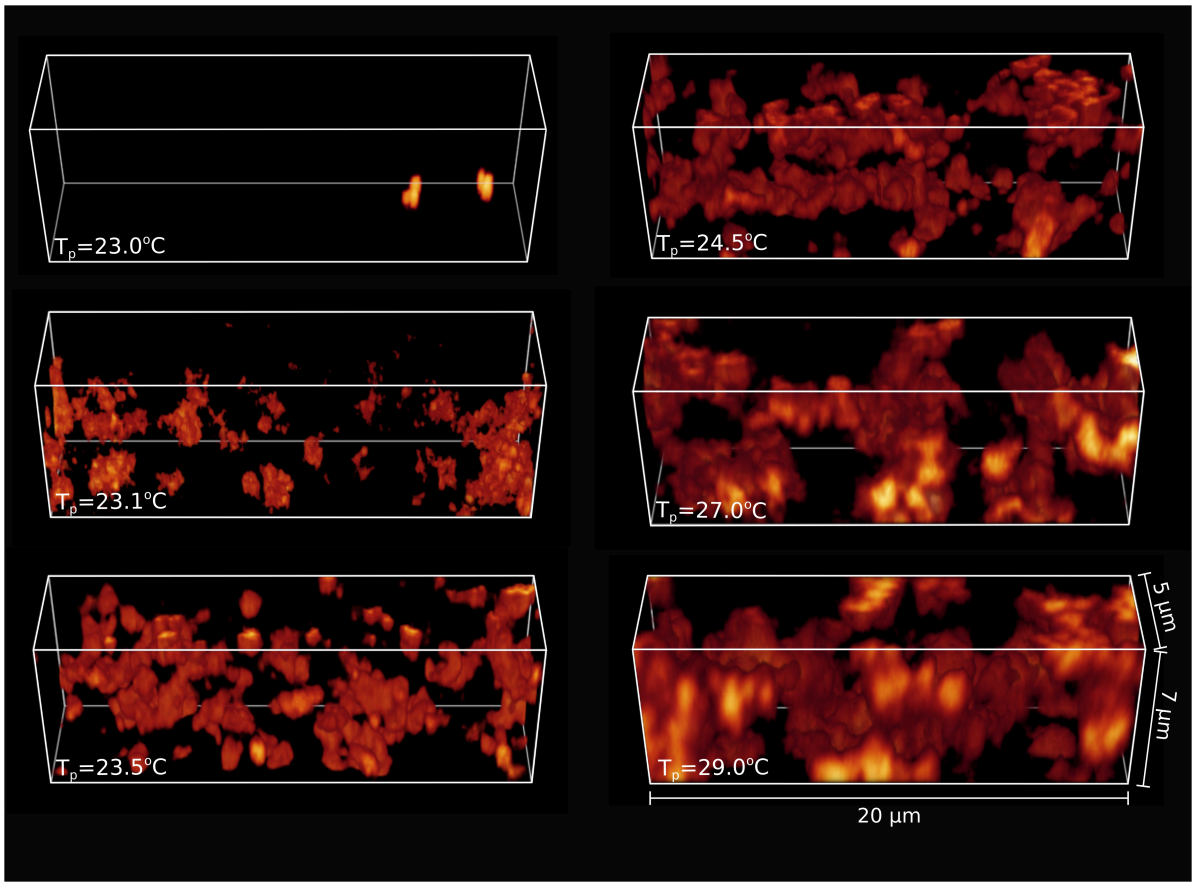

Figure 6: 3D STED images of BA-ATTO647N distributions within bulk PNIPAM gels prepared at different temperatures. The intensities from the surrounding matrix has been thresholded out in each image to selectively visualize the distribution of highly crosslinked domains within the subvolume and highlight the increasing volume fraction and connectivity between the domains with preparation temperature.

in bulk PNIPAM gels prepared at different temperatures. Each of the STED images has been thresholded to selectively depict the distribution of high crosslink density regions within a sub-volume, with the threshold value set to be above the average intensity observed within the matrix regions. The primary insight from these images is the connectivity of the higher crosslink density domains. This connectivity is determined by utilizing a density-based clustering non-parametric algorithm, DBSCAN,[45] to count the number of independent clusters within multiple subvolumes in gels at each preparation temperature (see Figure S5A of the

SI). Below preparation temperatures of 27^{o}C, isolated higher crosslink density domains are observed. A single continuously connected entity comprised by regions of higher crosslink density is only evident in the images of gels prepared at 27.0^{o}C and 29.0^{o}C. An increasing incidence of connectivity with increasing preparation temperature is observed. This trend is accompanied by an increasing volume fraction of spatial heterogeneities (shown in Figure S5B of SI) within the network, and is consistent with the expected increased incidence of phase separation at higher polymerization temperatures.

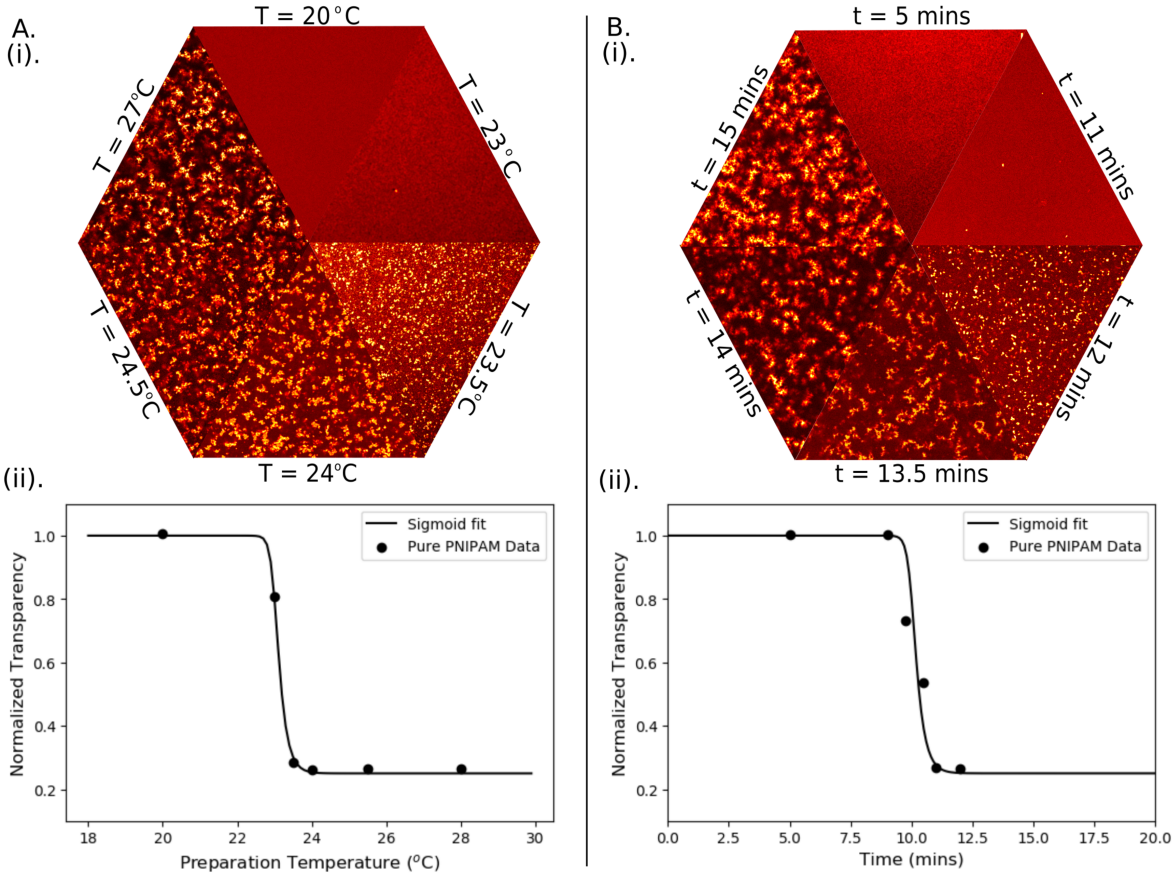

Figure 7: **(A)(i)** Evolution of microstructure in BMA-ATTO647N tagged bulk PNIPAM gels prepared at different temperatures for 60 mins. **(ii)** Variation in normalized transmittance exhibited by pristine hydrogels prepared at different preparation temperatures for 60 mins. **(B)(i)** Evolution of microstructure in BMA-ATTO647N tagged bulk PNIPAM gels with quench times, during preparation at 27^{o}C. Quenching was achieved by placing the reaction mixture in a temperature bath maintained at 18^{o}C for the remainder of the preparation time. **(B)(ii)** Variation in normalized transmittance exhibited by untagged hydrogels quenched at different times during gel preparation at T_p = 27^{o}C. Hexagonal side length is equal to 125μm.

The increased incidence of spatial heterogeneities manifests itself at macroscopic length

scales in the form of reduced optical clarity in bulk PNIPAM gel system. The dependence of gel transparency as a function of preparation temperature has been shown to possess a sigmoidal signature.[23] Figure 7A(i) shows LSCM images of the final dye tagged distributions as a function of preparation temperature in PNIPAM bulk gels containing BMA-ATTO647N. Similar to the case of BA-ATTO647N tagged gels, a transition from isolated highly crosslinked domains at lower preparation temperatures to increasingly connected spatial heterogeneities at higher preparation temperatures is observed. The increasing volume fraction and dimensions of the scattering domains in the network correlates well with the sigmoidal decrease in transparency for the untagged bulk PNIPAM gel system shown in Figure 7A(ii). This correlation confirms that the formation of spatial heterogeneities within PNIPAM gels containing trace amounts of dye tagged monomer is primarily driven by the majority NIPAM and BIS monomers.

To capture how the morphology of spatial heterogeneities evolve in time, various reaction mixtures maintained at 27^oC were quenched at intermediate times to 18^oC and maintained at the latter temperature for the remainder of the gelation process. Figure 7B(i) shows BMA-ATTO647N distributions within these gels. The similarities between the progression of microstructural features in preparation temperatures and quench times is striking. Figure 7B(ii) demonstrates that the similarity in morphology is further reflected in the sigmoidal nature of the transparency for bulk untagged PNIPAM gels as a function of quench times.

The aforementioned similarity between the progression of structure and transparency in temperature and time highlights the important role that the spatiotemporal evolution of temperature across the reaction mixture plays in determining the structure of spatial heterogeneities in thermosensitive gels. A side observation serves as a case in point; even with precisely controlled polymerization bath temperatures, the morphology of the gels close to the substrate in contact with the isothermal bath differs from the bulk morphology of the gel. For example, in gels prepared at 27^oC, the morphology within $\sim 1\mu$m of the substrate resembles that of thin gel films previously reported in the literature.[42] The thin film morphology results

are, in turn, consistent with observations that the properties of thin PNIPAM films such as the volume phase transition temperature can deviate significantly from those of bulk films.[46]

Finally, we place our results in the broader context of investigating the structure and origin of spatial heterogeneities in thermosensitive gels. The ability to directly image dye tagged monomer distributions with greater resolution while varying their hydrophobicity and reaction rate constant has implications beyond the results shown here. Previously, experimental parameters such as temperature[47,48] and concentration of monomers[4,18,49–52] were varied to provide insights into the origin of spatial heterogeneities. A recent review[2] makes the case that these results do not decouple the impact of kinetic and phase separation on crosslink distributions. The use of dye functionalized crosslinkers facilitates this decoupling by enabling the direct visualization of the impact on local distribution of the tagged monomers.

As an example of how the combined use of super resolution microscopy and tagged monomers with a library of reactivity rate constants and solubilities can improve, challenge and support existing models for the origin of spatial hetereogeneities in gels, we examine the implications of our morphological findings for the 2008 LSCM model for PNIPAM. As per this model, which is primarily based on LSCM and scattering studies[22,23] as well as spectroscopic studies,[24] the structure is formed in two stages. At preparation temperatures that correspond to the initial plateau of the sigmoidal transition, swollen random copolymer coils form and subsequently undergo one step crosslinking, or macrogelation, to form a swollen homogeneous network. At polymerization temperatures above the LCST, globular copolymer chains form, are initially dissolved in aqueous medium and undergo phase separation to form droplets. In the second stage, microgels are formed via crosslinking within the droplets; these microgels are described as co-existing with newly formed chains and droplets. Subsequently, the microgels, droplets and globular copolymer chains phase separate from water into a sponge-like domain. Gelation of the polymer rich sponge-like domain results in the formation of the final gel.

Many of the imaging results in this paper offer strong support of the 2008 LSCM model.

At lower preparation temperatures, the morphology recorded is homogeneous for all times. At higher polymerization temperatures and after sufficient time, *e.g.* 13.5 minutes for a polymerization temperature of 27^{o}C in Figure 7, morphologies characteristic of phase separation are seen. The central role of phase separation in the 2008 LSCM model rests in part on work by Tanaka and co-workers,[27] who argued that the heat generated from polymerization within the reaction mixture is sufficient to push the local temperature above the LCST of the system. The two stages of the 2008 LSCM model imply that these excursions in temperature are initially restricted to isolated local volumes in the reaction mixture and later are global in extent. The latter is consistent with experimental evidence that the global temperature of the reaction mixture increases with time before peaking and decreasing back to the preparation temperature.[47] The peak global temperatures exceed the LCST for higher preparation temperatures, and the length of time during which the reaction mixture temperature exceeds the LCST increases with preparation temperature. These observations explain not just the formation of the connected fractal networks but also the increasing dimensions of the polymer rich spatial heterogeneities in the tagged gels prepared at 24^{o}C, 24.5^{o}C and 27^{o}C.

Other results in this paper represent new evidence in support of the 2008 LSCM model. The images at intermediate temperatures such as 23^{o}C and 23.5^{o}C, as well as those of shorter times at higher polymerization temperatures, *e.g.* below 11 minutes for 27^{o}C, are the first direct visualization of the isolated higher crosslink domains (see Figure 7) proposed in the first stage. The difference in the number of isolated domains between 23^{o}C and 23.5^{o}C can be attributed to the greater incidence of local excursions with increasing preparation temperature. The observation of isolated higher crosslink domains is noteworthy as it establishes that local excursions across the LCST are not always accompanied by global excursions across the LCST, as the spectroscopic studies imply.[24]

Finally, certain results in this paper establish that the 2008 LSCM model is incomplete. Two salient structural features deviate from the 2008 LSCM model. First, the interface

between the polymer rich and water rich regions, although distinct, is not found to be associated with a discontinuity in the crosslink densities of the regions that it separates. A related observation is that while isolated domains of higher crosslink density are observed at intermediate times at higher polymerization temperatures, at longer times, features with similar size and crosslink density do not display distinct boundaries. Second, the regions of higher crosslink density within the polymer rich heterogeneities are on average centrally located, with the crosslink density monotonically decreasing towards the interface. Furthermore, monomers with different reaction rate constants that are tagged with the same dye, show different spatial distributions. All these structural features can be explained by incorporating the impact of differences in reactivity rate constants into the 2008 LSCM model; the model currently ascribes the origin of spatial heterogeneities solely to phase separation based phenomena. As noted in a review on the origins of nanostructured inhomogeneities in polymer network gels,[2] much of the experimental work used to validate the various models, such as the impact of varying temperature or crosslinker content, is often discussed and evaluated with a particular model in mind. Our results provide direct visual evidence that a combination of the proposed mechanisms can simply explain the resultant morphologies.

Conclusion

In summary, we have combined the use of super resolution microscopy and a library of dye tagged multifunctional monomers whose hydrophilicity and reactivity rate constants can be easily varied, to advance the current understanding behind the origins and structure of spatial heteorogeneities in PNIPAM networks. The introduction of these dye tagged monomers enables the direct visualization of how spatial heterogeneities vary as a function of polymerization quench times, and the impact of phase separation and reaction rate constant differences on the local distribution of crosslinks. The superior resolution offered by 3D STED microscopy provides new morphological insights into the nature of the interface between the

polymer rich regions and the surrounding 'matrix', the connectivity of the polymer rich domains and the distribution of crosslink densities within these domains. These results provide the impetus for the formulation of an updated and more general model of spatial heterogeneities in thermosensitive gels that extends beyond the current model of a sponge-like network of heterogeneities.

Acknowledgments

This work is based in part upon work supported by the National Science Foundation under grant no. 1654599 and instrumentation acquired under grant no. 1725984. Acknowledgment is made to the Donors of the American Chemical Society Petroleum Research Fund for partial support of this research. We thank Prof. Chang Ryu and Prof. Edmund Palermo for graciously allowing use of their laboratory facilities. We also thank Alexander Yepikhin for assistance in the dye coupling.

Supporting Information

Full chemical names and sources of chemicals used; chemical structures of dyes and linkers used; brief description of relevant aspects of 3D STED microscopy; multicolor LSCM images of dye functionalized BMA and APMA monomers; additional line profiles of dye tagged monomers in polymer rich heterogeneities; line profiles of dye tagged monomers across polymer rich heterogeneities; and plots of variation of number of polymer rich domains and their volume fraction as a function of preparation temperature.

References

(1) Gu, Y.; Zhao, J.; Johnson, J. A. A (Macro)Molecular-Level Understanding of Polymer Network Topology. *Trends in Chemistry* **2019**, *1*, 318 – 334.

(2) Seiffert, S. Origin of nanostructural inhomogeneity in polymer-network gels. *Polym. Chem.* **2017**, *8*, 4472–4487.

(3) Lindemann, B.; Schroeder, U. P.; Oppermann, W. Influence of the Cross-Linker Reactivity on the Formation of Inhomogeneities in Hydrogels. *Macromolecules* **1997**, *30*, 4073–4077.

(4) Nie, J.; Du, B.; Oppermann, W. Influence of Formation Conditions on Spatial Inhomogeneities in Poly(N-isopropylacrylamide) Hydrogels. *Macromolecules* **2004**, *37*, 6558–6564.

(5) Kizilay, M. Y.; Okay, O. Effect of swelling on spatial inhomogeneity in poly(acrylamide) gels formed at various monomer concentrations. *Polymer* **2004**, *45*, 2567–2576.

(6) Kizilay, M. Y.; Okay, O. Effect of initial monomer concentration on spatial inhomogeneity in poly(acrylamide) gels. *Macromolecules* **2003**, *36*, 6856–6862.

(7) Takata, S. I.; Norisuye, T.; Shibayama, M. Preparation temperature dependence and effects of hydrolysis on static inhomogeneities of poly(acrylamide) gels. *Macromolecules* **1999**, *32*, 3989–3993.

(8) Stein, R. S.; Soni, V. K.; Yang, H.; Erman, B. *Biol. Synth. Polym. Networks*; Springer Netherlands, 1988; pp 383–400.

(9) Shibayama, M.; Ikkai, F.; Shiwa, Y.; Rabin, Y. Effect of degree of cross-linking on spatial inhomogeneity in charged gels. I. Theoretical predictions and light scattering study. *J. Chem. Phys.* **1997**, *107*, 5227–5235.

(10) Liu, R.; Oppermann, W. Spatial inhomogeneities of polystrene gels prepared from semidilute solutions. *Macromolecules* **2006**, *39*, 4159–4167.

(11) Gundogan, N.; Okay, O.; Oppermann, W. Swelling, Elasticity and Spatial Inhomogeneity of Poly(N,N-dimethylacrylamide) Hydrogels Formed at Various Polymer Concentrations. *Macromol. Chem. Phys.* **2004**, *205*, 814–823.

(12) Mallam, S.; Horkay, F.; Hecht, A. M.; Geissler, E. Scattering and Swelling Properties of Inhomogeneous Polyacrylamide Gels. *Macromolecules* **1989**, *22*, 3356–3361.

(13) Deen, G. R.; Alsted, T.; Richtering, W.; Pedersen, J. S. Synthesis and characterization of nanogels of poly(N-isopropylacrylamide) by a combination of light and small-angle X-ray scattering. *Phys. Chem. Chem. Phys.* **2011**, *13*, 3108–3114.

(14) Mendes, E.; Lindner, P.; Buzier, M.; Boué, F.; Bastide, J. Experimental evidence for inhomogeneous swelling and deformation in statistical gels. *Phys. Rev. Lett.* **1991**, *66*, 1595–1598.

(15) Mendes, E.; Schosseler, F.; Isel, F.; Boué, F.; Bastide, J.; Candau, S. J. A SANS Study of Uniaxially Elongated Polyelectrolyte Gels. *EPL (Europhysics Lett.)* **1995**, *32*, 273.

(16) Shibayama, M.; Kawakubo, K.; Ikkai, F.; Imai, M. Small-angle neutron scattering study on charged gels in deformed state. *Macromolecules* **1998**, *31*, 2586–2592.

(17) Norisuye, T.; Masui, N.; Kida, Y.; Ikuta, D.; Kokufuta, E.; Ito, S.; Panyukov, S.; Shibayama, M. Small angle neutron scattering studies on structural inhomogeneities in polymer gels: Irradiation cross-linked gels vs chemically cross-linked gels. *Polymer* **2002**, *43*, 5289–5297.

(18) Takata, S. I.; Norisuye, T.; Shibayama, M. Small-angle neutron-scattering study on preparation temperature dependence of thermosensitive gels. *Macromolecules* **2002**, *35*, 4779–4784.

(19) Koizumi, S.; Monkenbusch, M.; Richter, D.; Schwahn, D.; Farago, B. Concentration

fluctuations in polymer gel investigated by neutron scattering: Static inhomogeneity in swollen gel. *J. Chem. Phys.* **2004**, *121*, 12721–12731.

(20) Norisuye, T.; Kida, Y.; Masui, N.; Tran-Cong-Miyata, Q.; Maekawa, Y.; Yoshida, M.; Shibayama, M. Studies on Two Types of Built-in Inhomogeneities for Polymer Gels: Frozen Segmental Concentration Fluctuations and Spatial Distribution of Cross-Links. *Macromolecules* **2003**, *36*, 6202–6212.

(21) Stieger, M.; Richtering, W.; Pedersen, J. S.; Lindner, P. Small-angle neutron scattering study of structural changes in temperature sensitive microgel colloids. *The Journal of Chemical Physics* **2004**, *120*, 6197–6206.

(22) Hirokawa, Y.; Jinnai, H.; Nishikawa, Y.; Okamoto, T.; Hashimoto, T. Direct Observation of Internal Structures in Poly(N-isopropylacrylamide) Chemical Gels. *Macromolecules* **1999**, *32*, 7093–7099.

(23) Hirokawa, Y.; Okamoto, T.; Kimishima, K.; Jinnai, H.; Koizumi, S.; Aizawa, K.; Hashimoto, T. Sponge-like Heterogeneous Gels: Hierarchical Structures in Poly(N-isopropylacrylamide) Chemical Gels As Observed by Combined Scattering and Confocal Microscopy Method. *Macromolecules* **2008**, *41*, 8210–8219.

(24) Park, Y.; Hashimoto, C.; Hashimoto, T.; Hirokawa, Y.; Jung, Y. M.; Ozaki, Y. Reaction-Induced Self-Assembly of Gel Structure: A New Insight into Chemical Gelation Process of N-Isopropylacrylamide as Studied by Two-Dimensional Infrared Correlation Spectroscopy. *Macromolecules* **2013**, *46*, 3587–3602.

(25) Baddeley, D.; Bewersdorf, J. Biological Insight from Super-Resolution Microscopy: What We Can Learn from Localization-Based Images. *Annual Review of Biochemistry* **2018**, *87*, 965–989.

(26) Orakdogen, N.; Kizilay, M. Y.; Okay, O. Suppression of inhomogeneities in hydrogels formed by free-radical crosslinking copolymerization. *Polymer* **2005**, *46*, 11407 – 11415.

(27) Matsuo, E. S.; Orkisz, M.; Sun, S.-T.; Li, Y.; Tanaka, T. Origin of Structural Inhomogeneities in Polymer Gels. *Macromolecules* **1994**, *27*, 6791–6796.

(28) Panyukov, S.; Rabin, Y. Statistical physics of polymer gels. *Physics Reports* **1996**, *269*, 1 – 131.

(29) Panyukov, S.; Rabin, Y. Polymer Gels: Frozen Inhomogeneities and Density Fluctuations. *Macromolecules* **1996**, *29*, 7960–7975.

(30) Tobita, H.; Hamielec, A. Crosslinking kinetics in polyacrylamide networks. *Polymer* **1990**, *31*, 1546 – 1552.

(31) Naghash, H. J.; Okay, O. Formation and structure of polyacrylamide gels. *Journal of Applied Polymer Science* **1996**, *60*, 971–979.

(32) Okay, O. Kinetic modelling of network formation and properties in free-radical crosslinking copolymerization. *Polymer* **1994**, *35*, 796 – 807.

(33) Patras, G.; Qiao, G. G.; Solomon, D. H. Controlled Formation of Microheterogeneous Polymer Networks: Influence of Monomer Reactivity on Gel Structure. *Macromolecules* **2001**, *34*, 6396–6401.

(34) Hell, S. W. Nanoscopy with Focused Light (Nobel Lecture). *Angewandte Chemie International Edition* **2015**, *54*, 8054–8066.

(35) Harke, B.; Ullal, C. K.; Keller, J.; Hell, S. W. Three-Dimensional Nanoscopy of Colloidal Crystals. *Nano Letters* **2008**, *8*, 1309–1313.

(36) Ullal, C. K.; Schmidt, R.; Hell, S. W.; Egner, A. Block Copolymer Nanostructures Mapped by Far-Field Optics. *Nano Letters* **2009**, *9*, 2497–2500.

(37) Chapman, D. V.; Du, H.; Lee, W. Y.; Wiesner, U. B. Optical super-resolution microscopy in polymer science. *Progress in Polymer Science* **2020**, *111*, 101312.

(38) Qiang, Z.; Wang, M. 100th Anniversary of Macromolecular Science Viewpoint: Enabling Advances in Fluorescence Microscopy Techniques. *ACS Macro Letters* **2020**, *9*, 1342–1356.

(39) Conley, G. M.; Nöjd, S.; Braibanti, M.; Schurtenberger, P.; Scheffold, F. Superresolution microscopy of the volume phase transition of pNIPAM microgels. *Colloids and Surfaces A: Physicochemical and Engineering Aspects* **2016**, *499*, 18 – 23.

(40) Gelissen, A. P. H.; Oppermann, A.; Caumanns, T.; Hebbeker, P.; Turnhoff, S. K.; Tiwari, R.; Eisold, S.; Simon, U.; Lu, Y.; Mayer, J.; Richtering, W.; Walther, A.; Wöll, D. 3D Structures of Responsive Nanocompartmentalized Microgels. *Nano Letters* **2016**, *16*, 7295–7301.

(41) Bergmann, S.; Wrede, O.; Huser, T.; Hellweg, T. Super-resolution optical microscopy resolves network morphology of smart colloidal microgels. *Phys. Chem. Chem. Phys.* **2018**, *20*, 5074–5083.

(42) Karanastasis, A. A.; Zhang, Y.; Kenath, G. S.; Lessard, M. D.; Bewersdorf, J.; Ullal, C. K. 3D mapping of nanoscale crosslink heterogeneities in microgels. *Mater. Horiz.* **2018**, *5*, 1130–1136.

(43) Karanastasis, A. A.; Kenath, G. S.; Sundararaman, R.; Ullal, C. K. Quantification of functional crosslinker reaction kinetics via super-resolution microscopy of swollen microgels. *Soft Matter* **2019**, *15*, 9336–9342.

(44) Zanetti-Domingues, L. C.; Martin-Fernandez, M. L.; Needham, S. R.; Rolfe, D. J.; Clarke, D. T. A Systematic Investigation of Differential Effects of Cell Culture Substrates on the Extent of Artifacts in Single-Molecule Tracking. *PLOS ONE* **2012**, *7*, 1–13.

(45) Ester, M.; Kriegel, H.-P.; Sander, J.; Xu, X. A Density-Based Algorithm for Discovering

Clusters in Large Spatial Databases with Noise. Proceedings of the Second International Conference on Knowledge Discovery and Data Mining. 1996; p 226–231.

(46) Harmon, M. E.; Jakob, T. A. M.; Knoll, W.; Frank, C. W. A Surface Plasmon Resonance Study of Volume Phase Transitions in N-Isopropylacrylamide Gel Films. *Macromolecules* **2002**, *35*, 5999–6004.

(47) Kara, S.; Okay, O.; Pekcan, O. Real-time temperature and photon transmission measurements for monitoring phase separation during the formation of poly(N-isopropylacrylamide) gels. *Journal of Applied Polymer Science 86*, 3589–3595.

(48) Sayil, C.; Okay, O. Macroporous poly(N-isopropyl)acrylamide networks: formation conditions. *Polymer* **2001**, *42*, 7639 – 7652.

(49) Durmaz, S.; Okay, O. Inhomogeneities in poly(acrylamide) gels: position-dependent elastic modulus measurements. *Polymer Bulletin* **2001**, *46*, 409–418.

(50) Kizilay, M. Y.; Okay, O. Effect of hydrolysis on spatial inhomogeneity in poly(acrylamide) gels of various crosslink densities. *Polymer* **2003**, *44*, 5239 – 5250.

(51) Orakdogen, N.; Okay, O. Correlation between crosslinking efficiency and spatial inhomogeneity in poly(acrylamide) hydrogels. *Polymer Bulletin* **2006**, *57*, 631–641.

(52) Cerid, H.; Okay, O. Minimization of spatial inhomogeneity in polystyrene gels formed by free-radical mechanism. *European Polymer Journal* **2004**, *40*, 579 – 587.

For Table of Contents Only

Super resolution imaging of spatial heterogeneities in model thermosensitive hydrogels with implications for their origins

Gopal S. Kenath, Apostolos A. Karanastasis, Chaitanya K. Ullal